

# Viscous Fluid Models of Cosmic Acceleration in FRW Spacetime Using MCMC Constraints

Mohit Thakre<sup>1</sup>, Praveen Kumar Dhankar<sup>2</sup>, Behnam Pourhassan<sup>3,5,6</sup>, and Safiqul Islam<sup>4</sup>

<sup>1,2</sup>Symbiosis Institute of Technology, Nagpur Campus, Symbiosis International (Deemed University), Pune 440008, Maharashtra, India. <sup>1</sup>Email: mohitthakre100@gmail.com; <sup>2</sup>Email: pkumar6743@gmail.com

<sup>3</sup>School of Physics, Damghan University, Damghan, 3671641167, Iran. <sup>3</sup>Email: b.pourhassan@du.ac.ir

<sup>5</sup>Center for Theoretical Physics, Khazar University, 41 Mehseti Street, Baku, AZ1096, Azerbaijan.

<sup>6</sup>Centre of Research Impact and Outcome, Chitkara University, Punjab, Rajpura, 140417, India.

<sup>4</sup>Department of Basic Sciences, General Administration of Preparatory Year, King Faisal University, P.O. Box 400, Al Ahsa 31982, Saudi Arabia & Department of Mathematics and Statistics, College of Science, King Faisal University, P.O. Box 400, Al Ahsa 31982, Saudi Arabia. <sup>4</sup>Email: sislam@kfu.edu.sa

## Abstract

This study combines theoretical advancements with observational limitations to investigate the cosmological implications of a bulk viscous modified Chaplygin gas (MCG) in a Friedmann–Robertson–Walker (FRW) in (3+1) dimensional spacetime framework. We provide analytical solutions for both viscous and non-viscous cases, pointing out variations in the energy density evolution, the Hubble parameter dynamics, and the deceleration parameter transitions. Bulk viscosity suppresses oscillations in structure creation, a well-known drawback of Chaplygin gas models in larger dimensions, as shown by a thorough perturbation analysis. Using the bulk viscosity coefficient and Hubble expansion parameter, which are incorporated by the total pressure and the appropriate pressure and by using energy momentum conservation law determined time time-dependent density. With the help of three conditions ( $\xi = 0$ ,  $\xi \neq 0$ , and we neglect both bulk viscosity and presence of Chaplygin gas, i.e  $A = 0$  and  $\xi = 0$ ) created three different models as the Hubble parameter is a function of redshift  $z$ . By applying the MCMC method to these models, we have gone through observational analysis by using the Hubble and BAO datasets.

## 1 Introduction

Characterizing the Universe from its initial high energy state through the structure building sequence to the current epoch of accelerated expansion is one of the main issues in modern cosmology. Our comprehension of early time dynamics and isotropization has long benefited from studies of anisotropic and viscous cosmological models [2, 5, 12, 26]. Other theoretical frameworks, such Chaplygin type fluids [1, 56, 62, 63] and modified gravity, offer complementary methods to solve cosmological conundrums and connect early and late time behavior [3, 4, 6, 13, 30]. Dissipative processes can affect global dynamics and possibly prevent singular behavior in idealized models, as demonstrated by fundamental studies into bulk viscous effects and isotropy [42, 47]. Theoretical models are anchored by observational probes like as direct Hubble parameter determinations, Type Ia supernovae, baryon acoustic oscillations (BAO), and precise measurements of the cosmic microwave background (CMB). The Universe’s large scale homogeneity and anisotropy have been limited by landmark CMB analyses and associated datasets, which have also placed strict limits on cosmological parameters [7, 35, 55, 58, 59]. The expansion history and geometry of spacetime are further constrained by independent observations of the Hubble parameter and BAO data [43, 84]. Collectively, these findings support

both minor adjustments to the concordance model and more drastic substitutes, and they offer the empirical foundation for testing Chaplygin gas models, viscous fluids, and modified gravity situations [32, 64–66]. The most straightforward explanation for late time acceleration is still the cosmological constant  $\Lambda$ . However, it suffers from conceptual issues, particularly the coincidence problem and fine tuning, which have led to a number of theoretical assessments and proposals [11, 48, 50, 53, 54, 82]. Different phenomenologies for cosmic acceleration and structure growth are provided by braneworld setups, tachyonic matter, and dynamical dark energy models (such as quintessence, phantom, and related scalar field constructions) [10, 21, 25, 57, 69, 70]. In parallel, geometric pathways to simulate dark energy behavior without utilizing a pure vacuum energy term are shown via holographic and modified gravity frameworks (such as  $f(R)$  and Gauss Bonnet inspired structures) [14, 15, 33, 68, 71]. An equation of state that interpolates between dust like and cosmological constant like behavior characterizes the Chaplygin gas family, which includes the original formulation as well as generalized and modified variants. This class of unified dark matter and dark energy models has been thoroughly studied [41, 60, 61, 72–74]. Chaplygin type fluids’ thermodynamic characteristics, phase space dynamics, and cosmological implications have been studied in a variety of settings, including brane world and higher dimensional scenarios as well as Gauss–Bonnet extensions [34, 37]. These studies demonstrate the flexibility of Chaplygin structures as well as the need for phenomenological adjustments to accommodate findings at intermediate redshifts. When modeling realistic cosmic fluids, dissipative processes, and bulk viscosity in particular, are physically well motivated extensions because expansion and perturbation dynamics are changed by viscous stresses that are naturally generated by deviations from local thermodynamic equilibrium [75]. The incorporation of bulk viscous terms into Kaluza Klein frameworks, FRW and anisotropic cosmologies, and different modified gravity settings has demonstrated that viscosity can function as an effective negative pressure and aid in smooth phase transitions or late time acceleration [16, 27, 45, 76]. An attractive unified image that can reduce data tensions while taking into account entropy formation and particle creation processes is produced by combining viscous effects with Chaplygin type equations of state [17, 18, 36, 78]. From a statistical and observational standpoint, more accurate datasets necessitate strong inference frameworks in order to investigate multidimensional parameter spaces and measure uncertainty. This endeavor relies heavily on Markov Chain Monte Carlo (MCMC) techniques, which allow for accurate posterior estimate even in cases when likelihood surfaces are multimodal or non Gaussian [22]. Modified Gauss–Bonnet or  $f(R)$  parametrizations have been tested against BAO and large scale structure data, probed interacting and holographic extensions, and viscous Chaplygin gas parameters have been constrained in recent work using MCMC and other Bayesian tools [46]. Additionally, growth rate measurements and matter power spectrum studies offer complementary handles on modified gravity and viscous signals [46]. Different theoretical frameworks have shaped the study of gravitational and cosmological models. In order to investigate dark energy–matter interactions, Cold Dark Matter models with a smooth component [79] were introduced. An alternate method of avoiding the Big Rip singularity was offered by the *hessence* dark energy model [80], subsequently rebuilt and examined with supernova data [81]. To further comprehend cosmic acceleration, a novel interaction between dark matter and generalized Chaplygin gas was proposed [83]. Modified gravity extensions were investigated using (2+1)-dimensional cosmological models in  $f(R, T)$  [28] gravity and further reinforced by advancements in time-scale inequalities mathematics [24]. Compact stellar configurations in  $f(R, T)$  gravity: an investigation [29] and These frameworks were extended by two-fluid cosmological models in scalar tensor theory [38]. Additionally, research on higher-dimensional spacetime’s weird quark matter [40] and Understanding cosmic evolution under modified gravity theories was greatly aided by divergence-free deceleration parameters in Weyl-type  $f(Q, T)$  gravity [23].

The study of bulk viscous cosmology with modified Chaplygin gas (MCG) in the FRW spacetime is motivated by the quest to resolve existing observational tensions in cosmology, particularly the discrepancies in the Hubble parameter, by adopting more realistic descriptions of cosmic fluids beyond the perfect-fluid framework [8, 9, 19, 77]. Nojiri and Odintsov [49] advanced an inhomogeneous equation of state to explain the universe’s transition across the phantom split. The MCG model, which naturally unifies dark matter and dark energy through its equation of state, gains further significance when bulk viscosity is included, as it accounts for dissipative processes and entropy production in cosmic evolution [51, 67]. The current study is situated in this framework, driven by the necessity to integrate these themes into a comprehensive model that reflects the dynamics of the universe from its earliest eras to its current accelerated expansion, all the while being consistent with the abundance of observational data [20, 39]. Paul [52] newly interrogated bulk viscosity’s thermodynamic genesis and associated it to nonequilibrium events in cosmic fluids. By using

MCMC statistical methods to limits model parameters, Joshi et al. [31] and Mune et al. [44] examined anisotropic Bianchi-type cosmologies in the view of modified  $f(R, T)$  gravity as a correlate to viscous and thermodynamic models. Together, these study provides reasonable illustration of how changed gravity frameworks and viscous effects can explain the accelerated dynamics of the universe. Sections 2 and 3 deals with the FRW line element and it's solution. Observational Data analysis with Hubble and BAO data is given in Section 4. MCMC plots are incorporated into this section with their significance. In Section 5 we define the Hubble and deceleration parameter. Stability analysis is incorporated in section 6 and Concluding remarks in section 7.

## 2 FRW line element

The following metric describes the Friedmann Robertson-Walker(FRW) universe in four-dimensional space-time. ([35]; [25]),

$$ds^2 = -dt^2 + a^2(t) \left( \frac{dr^2}{1 - kr^2} + r^2 d\theta^2 + r^2 \sin^2 \theta d\phi^2 \right), \quad (1)$$

and the scale factor is denoted by  $a(t)$ . With  $0 \leq \theta \leq \pi$  and  $0 \leq \phi < 2\pi$ , the  $\theta$  and  $\phi$  parameters are the standard azimuthal and polar angles of spherical coordinates. Comoving coordinates are the coordinates  $(t, r, \theta, \phi)$ . Additionally, the space's curvature is indicated by the constant  $k$ . Only the condition when  $k = 0$ , or flat space, is taken into consideration in this study. The Einstein equation is then provided by

$$R_{ij} - \frac{1}{2}g_{ij}R = T_{ij} + g_{ij}\Lambda, \quad (2)$$

where  $8\pi G = 1$  and  $c = 1$  were expected. Additionally, the following connection provides the energy-momentum tensor for the bulk viscous fluid and modified Chaplygin gas [3, 11, 12, 30, 74, 82].

$$T_{ij} = (\rho + \bar{p})u_i u_j - \bar{p}g_{ij}, \quad (3)$$

If the velocity vector is  $u^i$  and the energy density is  $\rho$ , with the normalization condition being  $u^i u_j = -1$ . Additionally, the following equations provide the total pressure and appropriate pressure, which incorporate the bulk viscosity coefficient  $\xi$  and the Hubble expansion parameter  $H = \dot{a}/a$ :

$$\bar{p} = p - 3\xi H, \quad (4)$$

and

$$p = \gamma\rho - \frac{A}{\rho^\alpha}, \quad (5)$$

With  $0 < \alpha \leq 1$  and  $A > 0$ . One of the most crucial numbers for characterizing the characteristics of dark energy theories is the equation of state parameter  $\gamma$ . Bulk viscosity is clearly represented by the parameter  $\xi$ , whereas the influence of the Chaplygin gas is represented by  $A$ . The dynamics of FRW cosmology with modified Chaplygin gas as the matter source were already developed in [59]. The eigenvalues of the linearized Jacobi matrix for the exceptional situation  $\alpha = 0.6$  were then evaluated in order to study the nature of the critical points. In this paper, we extend the earlier work [59] to incorporate the bulk viscous coefficient and analyze the exceptional situation  $\alpha = 0.5$ .

In that case the Friedmann equations are given by

$$\left( \frac{\dot{a}}{a} \right)^2 = \frac{\rho}{3}, \quad (6)$$

equation (6) can be written as

$$H^2 = \frac{\rho}{3} \quad (7)$$

and

$$2\frac{\ddot{a}}{a} + \left( \frac{\dot{a}}{a} \right)^2 = -\bar{p}, \quad (8)$$

where the derivative with regard to the cosmic time  $t$  is indicated by the dot. The following is the energy momentum conservation law:

$$\dot{\rho} + 3\frac{\dot{a}}{a}(\rho + \bar{p}) = 0. \quad (9)$$

equation (8) can be written as

$$\dot{\rho} + 3H(\rho + \bar{p}) = 0. \quad (10)$$

Using the above equations, we attempt to determine the time-dependent density in the next section.

### 3 Solution of a line element

Using the conservation relation (9) and Eqs.(4),(5) and (6), we have

$$\dot{\rho} + \sqrt{3}(\gamma + 1)\rho^{\frac{3}{2}} - 3\xi\rho - \sqrt{3}A = 0. \quad (11)$$

Case (I) :  $\xi = 0$ , then one can extract the energy density as a function of the scale factor [59].

$$\rho(a) = \left[ \frac{1}{\gamma + 1} \left( A + \frac{d}{\sqrt{a^{9(\gamma+1)}}} \right) \right]^{\frac{2}{3}}, \quad (12)$$

where  $d$  is an integration constant.

Put the value of equation (12) in equation (7), we get

$$H(a) = \frac{1}{\sqrt{3}} \left[ \frac{1}{\gamma + 1} \left( A + \frac{d}{\sqrt{a^{9(\gamma+1)}}} \right) \right]^{\frac{1}{3}}, \quad (13)$$

as

$$a = (1 + z)^{-1}$$

equation (12) can be written as

$$\rho(z) = \left[ \frac{1}{\gamma + 1} \left( A + d(1 + z)^{3\sqrt{\gamma+1}} \right) \right]^{\frac{2}{3}}, \quad (14)$$

Put equation (14) in (7) then we get,

$$H(z) = \frac{1}{\sqrt{3}} \left[ \frac{1}{\gamma + 1} \left( A + d(1 + z)^{3\sqrt{\gamma+1}} \right) \right]^{\frac{1}{3}}, \quad (15)$$

Case(II) :  $\xi \neq 0$  (Constant)

In this case, we adhere to the specific  $\rho$  from previously provided by Saadat and Pourhassan.

$$\rho = \frac{B}{t^2} + \frac{F}{t} + ht + Ee^{bt}, \quad (16)$$

where the constants  $B$ ,  $F$ ,  $h$ ,  $E$ , and  $b$  should be determined. Substituting relation (16) into Eq. (11), we get

$$0 = \frac{d}{dt} \left[ \frac{B}{t^2} + \frac{F}{t} + ht + Ee^{bt} \right] + \sqrt{3}(\gamma + 1) \left[ \frac{B}{t^2} + \frac{F}{t} + ht + Ee^{bt} \right]^{\frac{3}{2}} - 3\xi \left( \frac{B}{t^2} + \frac{F}{t} + ht + Ee^{bt} \right) - \sqrt{3}A$$

By comparing both sides, gives us the following coefficients:

$$h = \sqrt{3}A, \quad (17)$$

$$B = \frac{4}{3}(\gamma + 1)^{-2}, \quad (18)$$

$$F = 2\xi(\gamma + 1)^{-2}, \quad (19)$$

$$E = \frac{(\gamma + 1)^2}{4} \left[ \frac{8\sqrt{3}\xi^2}{(\gamma + 1)^3} - \frac{3(\gamma + 1)^4}{16\xi^2} \right], \quad (20)$$

$$b = \frac{\xi[\sqrt{3}\xi(\gamma + 1)(A(\gamma + 1) - \frac{9}{2}\xi^3) + \frac{27}{32}(\gamma + \frac{1}{8}) + \frac{9}{16}\xi^4 + \mathcal{O}(\gamma^n)]}{8(\gamma + 1)(\sqrt{3}\xi^4 - \frac{3}{128}(\gamma + 1)^7)}, \quad (21)$$

where,

$$\mathcal{O}(\gamma^n) \equiv \frac{189}{64}\gamma^2 + \frac{189}{32}\gamma^3 + \frac{945}{128}\gamma^4 + \frac{189}{32}\gamma^5 + \frac{189}{64}\gamma^6 + \frac{27}{32}\gamma^7 + \frac{27}{256}\gamma^8. \quad (22)$$

After putting all the values of the arbitrary constant in Eq. (16), we get

$$\rho = \frac{4}{3(\gamma + 1)^2 t^2} + \frac{2\xi}{(\gamma + 1)^2 t} + \sqrt{3}At + Y_1 e^{Y_2} \quad (23)$$

where we define,

$$\begin{aligned} Y_1 &= \frac{(\gamma + 1)^2}{4} \left[ \frac{8\sqrt{3}\xi^2}{(\gamma + 1)^3} - \frac{3(\gamma + 1)^4}{16\xi^2} \right] \\ Y_2 &= Y_3 \left[ 8(\gamma + 1) \left( \sqrt{3}\xi^4 - \frac{3(\gamma + 1)^7}{128} \right) \right]^{-1} t \\ Y_3 &= \xi(Y_4 + \frac{9\xi^4}{16} + \mathcal{O}(\gamma^n)) \\ Y_4 &= Y_5 + \frac{27}{32}(\gamma + \frac{1}{8}) \\ Y_5 &= \sqrt{3}\xi(\gamma + 1)(A(\gamma + 1) - \frac{9}{2}\xi^3) \end{aligned}$$

from equation (7), the Hubble parameter can be written as

$$H = \sqrt{\frac{\rho}{3}} \quad (24)$$

The equation for red shift is  $1 + z = \frac{a_0}{a}$ , which also requires the normalized scale factor  $a_0 = 1$ . Following the establishment of the  $t - z$  relationship,  $t(z) = \frac{1}{n\alpha} \log(1 + (1 + z)^{-n})$  is obtained. To formulate  $\rho(z)$ , let consider

$$Y(z) = 1 + (1 + z)^{-n}$$

$$t(z) = \frac{1}{n\alpha} \log(Y(z))$$

$$\frac{1}{t} = \frac{n\alpha}{\log Y}$$

that implies,

$$\frac{1}{t^2} = \frac{n^2 \alpha^2}{(\log Y)^2}$$

for finding the values of  $\rho(z)$  we will find termwise

$$\frac{4}{3(\gamma + 1)^2 t^2} = \frac{4n^2 \alpha^2}{3(\gamma + 1)^2 (\log Y)^2}$$

$$\frac{2\xi}{(\gamma+1)^2 t} = \frac{2\xi n\alpha}{(\gamma+1)^2 (\log Y)^2}$$

$$\sqrt{3}AT = \frac{\sqrt{3}A}{n\alpha} \log Y$$

as,

$$Y_2 = Y_3 [8(\gamma+1)(\sqrt{3}\xi^4 - \frac{3}{128}(\gamma+1)^7)]^{-1} \frac{\log Y}{n\alpha}$$

Consider,

$$M = Y_3 [8(\gamma+1)(\sqrt{3}\xi^4 - \frac{3}{128}(\gamma+1)^7)]^{-1}$$

therefore,

$$Y_2 = \frac{M \log Y}{n\alpha}$$

$$e^{Y_2} = Y^{\frac{M}{n\alpha}}$$

from equation (23),

$$\rho(z) = \frac{4n^2\alpha^2}{3(\gamma+1)^2(\log Y)^2} + \frac{2\xi n\alpha}{(\gamma+1)^2(\log Y)^2} + \frac{\sqrt{3}A}{n\alpha} \log Y + Y_1 Y^{\frac{\Delta_1}{\Delta_2}} \quad (25)$$

where,

$$Y = 1 + (1+z)^{-n}$$

$$\frac{\Delta_1}{\Delta_2} = \frac{M}{n\alpha}$$

as we have,

$$H(a) = \frac{1}{\sqrt{3}} \rho^{\frac{1}{2}}$$

$$H(z) = \frac{1}{\sqrt{3}} [\rho(z)]^{\frac{1}{2}}$$

from eq(25), we get

$$H(z) = \frac{1}{\sqrt{3}} \left[ \frac{4n^2\alpha^2}{3(\gamma+1)^2(\log Y)^2} + \frac{2\xi n\alpha}{(\gamma+1)^2(\log Y)^2} + \frac{\sqrt{3}A}{n\alpha} \log Y + Y_1 Y^{\frac{\Delta_1}{\Delta_2}} \right]^{\frac{1}{2}} \quad (26)$$

Case (III): If we neglect both bulk viscosity and presence of Chaplygin gas, i.e  $A = 0$  and  $\xi = 0$ , our equation (11) becomes

$$\dot{\rho} + \sqrt{3}(\gamma+1)\rho^{\frac{3}{2}} = 0 \quad (27)$$

After solving equation (27), we get

$$\rho^{\frac{1}{2}} = \frac{2}{\sqrt{3}(\gamma+1)t} \quad (28)$$

therefore equation (28) becomes

$$\rho = \frac{4}{3(\gamma+1)^2 t^2}. \quad (29)$$

from equation (7), we get

$$H = \frac{2}{3(\gamma+1)t}. \quad (30)$$

Put the value of  $t$  in terms of  $z$ , we get

$$H(z) = \frac{2n\alpha}{3(\gamma + 1)\log(1 + (1 + z)^{-n})}. \quad (31)$$

equation (31) can be written as

$$H(z) = H_0 \left[ \frac{\log 2}{\log(1 + (1 + z)^{-n})} \right] \quad (32)$$

The findings of earlier studies [10, 59], where  $\rho \propto t^{-2}$  was established, are consistent with this. On the other hand,  $b < 0$  for a large bulk viscosity coefficient, which leads to the result  $\rho \propto \xi/t$ . Additionally, a constant negative energy density is obtained for the situation of infinitesimal  $\xi$ . Examining the density's late-time activity is intriguing. In such instance,  $\rho \sim Ee^{bt}$  can be stated since the final term of Eq. (16) is dominant. In the general situation, the energy density is a decreasing function of time, according to Eq. (16) with the coefficients (17)–(21). The following section discusses the Hubble expansion parameter, which likewise exhibits this tendency.

## 4 Observational data analysis

Let's use recent observational datasets, specifically the observed Hubble parameter measurements (OHD) and baryon acoustic oscillation (BAO) data, to test the model's feasibility. These datasets are especially helpful for verifying that the model is consistent with large-scale structure observations and offer complementary restrictions on the cosmic expansion history.

### 4.1 Hubble Data

The differential age (cosmic chronometer) methodology and the baryon acoustic oscillation (BAO) method are two popular methods in cosmology for estimating the Hubble parameter  $H(z)$  at a specific redshift [75, 76].

We use 30 observational measurements of  $H(z)$  in the redshift range of  $0.07 < z < 1.965$  in this work. As stated in

$$\chi_H^2 = \sum_{i=1}^{30} \frac{(H_{\text{th}} - H_{\text{obs}})^2}{\sigma_i^2} \quad (33)$$

where  $H_{\text{th}}$ ,  $H_{\text{obs}}$ , and  $\sigma_{H(z_i)}$  represent the standard error, the observed value, and the theoretical prediction of the Hubble parameter, respectively, for the 30 data points taken into consideration.

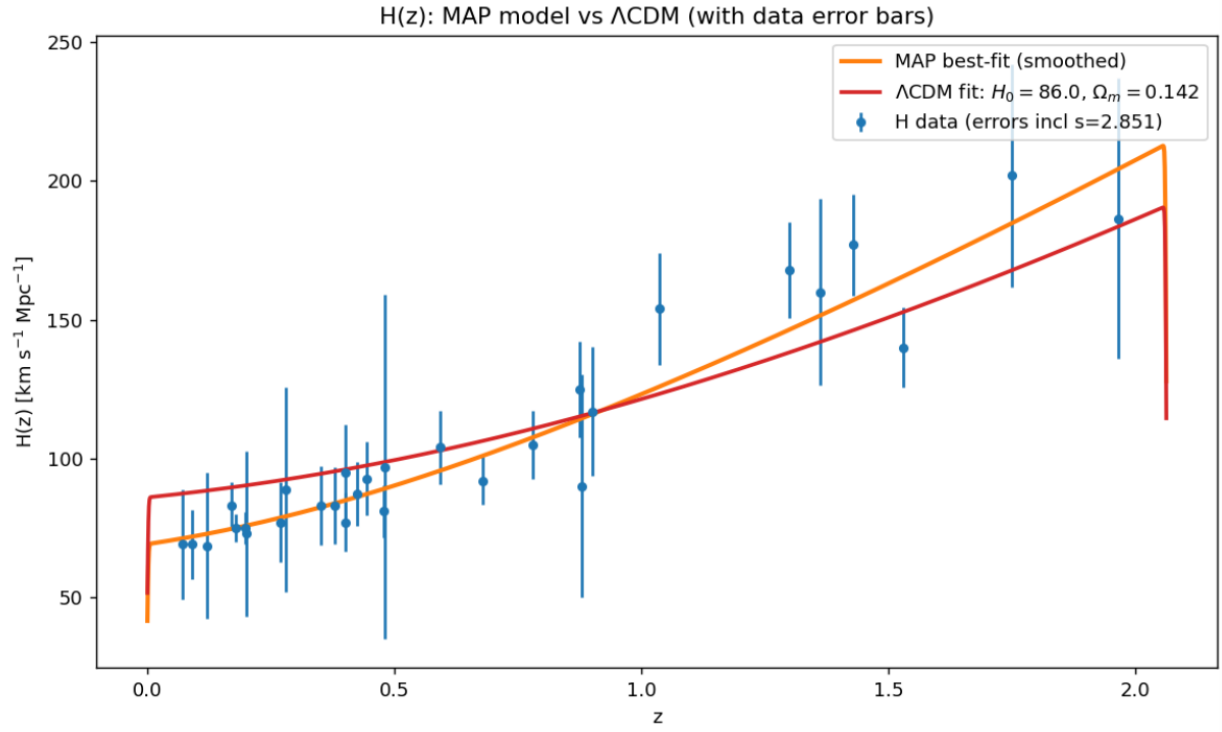


Figure 1: Hubble data Model(1) Error graph compare with  $\Lambda$  CDM model



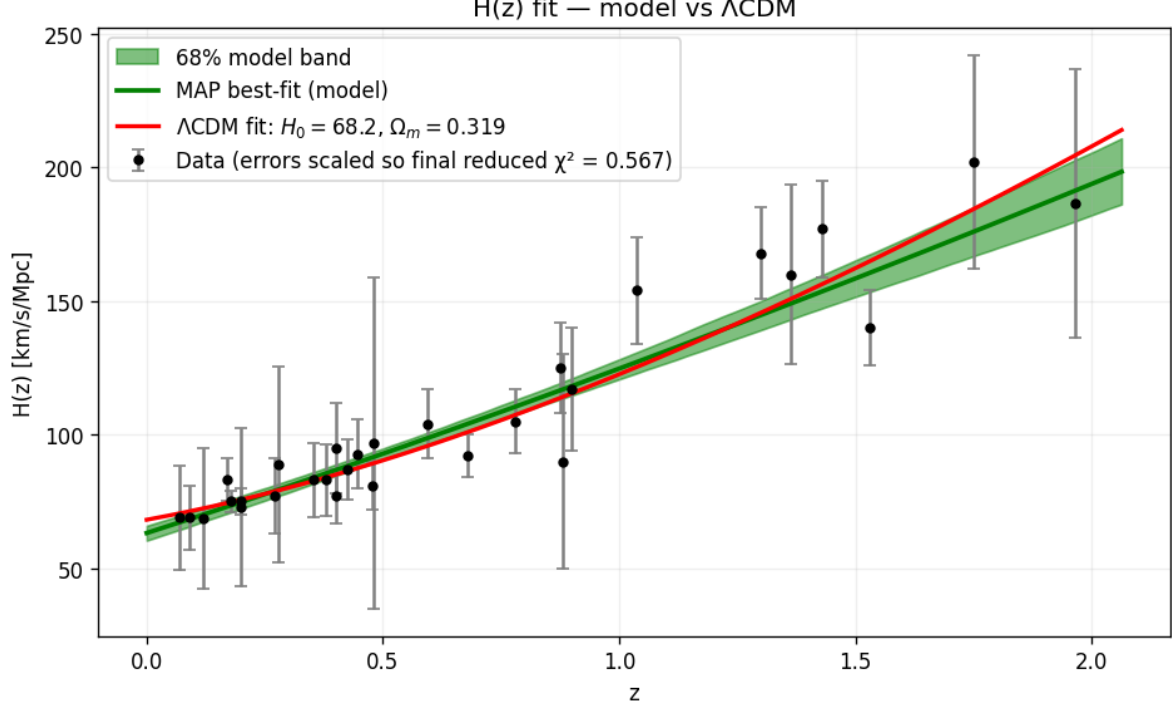


Figure 2: Hubble data Model(3) Error graph compare with  $\Lambda$  CDM model

Direct comparison with empirical Hubble parameter data can be used to evaluate the observational validation of our model. **Figure 1** presents our Model's predictions to demonstrate this comparison (1), displayed next to the traditional  $\Lambda$ CDM model (red curve), which is represented by the orange curve. The graphic includes 30 observational Hubble data points from the redshift interval  $0.07 < z < 2.0$ , each of which is shown with an accompanying error bar. Our model's MAP best-fit accurately captures the overall pattern of the observational data, especially at low to intermediate redshift values. The model curve stays well within the observational uncertainties, despite minor variations that show up at higher redshifts, demonstrating the model's resilience to actual data.

A different illustration of the evolution of the Hubble parameters using Model (3) is shown in Figure 1. The MAP best-fit is shown by the green curve in this case, with a 68% confidence band added (green shaded area), whereas the red line represents the  $\Lambda$ CDM fit. A major restriction in contemporary Hubble datasets is the growing measurement uncertainties at greater redshift, which are illustrated by the observational data points with their error bars. However, over the whole redshift range, our model predictions closely match the observable evidence as well as the  $\Lambda$ CDM trend. Since the majority of the data points fall inside one standard deviation, the error band's inclusion highlights the fit's statistical dependability even more.

When compared to the typical  $\Lambda$ CDM scenario, Figures 1 and 2 show that our models attain strong agreement with observable Hubble data. The capacity of our methodology to replicate the evolution of the Hubble parameters at all accessible redshifts indicates that it effectively represents the key characteristics of cosmic expansion. In the context of upcoming high-precision datasets, the slight variations seen at greater redshift might turn out to be important, possibly providing fresh perspectives on the fundamental physics of cosmic acceleration.

## 4.2 BAO data

By calculating the Hubble rate and/or distance combinations at distinct redshifts, Baryon Acoustic Oscillation (BAO) data offer a common benchmark that limits the late-time expansion. We use 17 observational measurements of  $H(z)$  from BAO in the redshift range  $0.106 < z < 2.340$  in this work. The BAO points that

have been directly reported as measurements of the Hubble parameter  $H(z)$  with uncertainties are used in this work. Our model's theoretical forecast for a parameter vector  $\phi$  is

$$H^{\text{th}}(z; \phi) \equiv H_0 E(z; \phi), \quad (34)$$

where  $E(z)$  is the dimensionless expansion function implied by the (3+1)-dimensional bulk viscous MCG dynamics. The comparison with data is performed through the standard  $\chi^2$  statistic

$$\chi_{\text{BAO}}^2(\phi) = \Delta_H^T \mathbf{C}_{\text{BAO}}^{-1} \Delta_H, \quad \Delta_H \equiv (H^{\text{th}}(z_i; \phi) - H_i^{\text{obs}})_{i=1}^{N_{\text{BAO}}}, \quad (35)$$

with  $\mathbf{C}_{\text{BAO}}$  the covariance matrix of the BAO  $H(z)$  data. For uncorrelated points, Eq. (35) reduces to

$$\chi_{\text{BAO}}^2(\phi) = \sum_{i=1}^{N_{\text{BAO}}} \frac{[H^{\text{th}}(z_i; \phi) - H_i^{\text{obs}}]^2}{\sigma_{H,i}^2}. \quad (36)$$

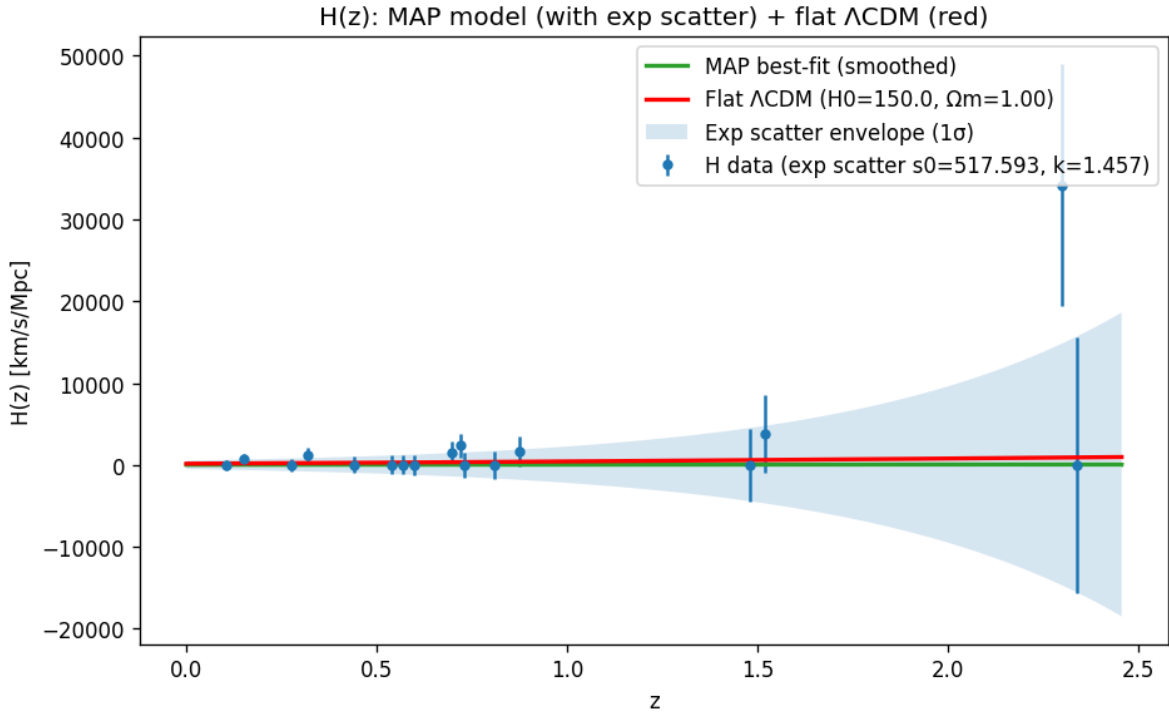


Figure 3: BAO data Model(1) Error graph compare with  $\Lambda$  CDM model

The option for intrinsic scatter In order to take into consideration potential extra dispersion that the cited mistakes do not account for (such as systematics that increase with redshift), we let an

The word "intrinsic scatter" is added to the measurement errors in quadrature.

$$\sigma_{H,i,\text{eff}}^2 = \sigma_{H,i}^2 + s_0^2 e^{2kz_i}, \quad (37)$$

for the purpose of evaluating Eq. (36) using  $\sigma_{H,i} \rightarrow \sigma_{H,i,\text{eff}}$ . The amplitude and redshift are controlled by the parameters  $s_0$  and  $k$ .

evolution of the additional scatter and are either profiled/marginalized over in the likelihood analysis or fixed by cross-validation.

**Estimating parameters and likelihood.** The BAO likelihood, assuming Gaussian errors, is  $\mathcal{L}_{\text{BAO}} \propto \exp[-\chi_{\text{BAO}}^2/2]$ . The highest

The reduced statistic  $\chi_\nu^2 = \chi_{\text{BAO}}^2/\nu$  with  $\nu = N_{\text{BAO}} - N_{\text{par}}$  summarizes goodness-of-fit. a-posteriori (MAP) or best-fit parameters are derived by minimizing  $\chi_{\text{BAO}}^2$  (or maximizing the full posterior if priors are employed). Results and comparison with  $\Lambda\text{CDM}$  Lambda CDM. The MAP prediction of our model (green line) and the  $1\sigma$  scatter envelope from Figure 3

Comparing the observational BAO  $H(z)$  data (points with error bars) with Eq. (37) (blue band). A flat  $\Lambda\text{CDM}$  fit is displayed in red for reference. While maintaining consistency with the observational errors, the model replicates the general trend and normalization of the BAO values throughout the sampled redshift range. The (2+1)-dimensional bulk viscous MCG framework captures the essential characteristics of late-time expansion while allowing for controlled variations that can be investigated with future, higher-precision BAO data, as evidenced by the close agreement with the  $\Lambda\text{CDM}$  curve.

### 4.3 Markov chain Monte Carlo

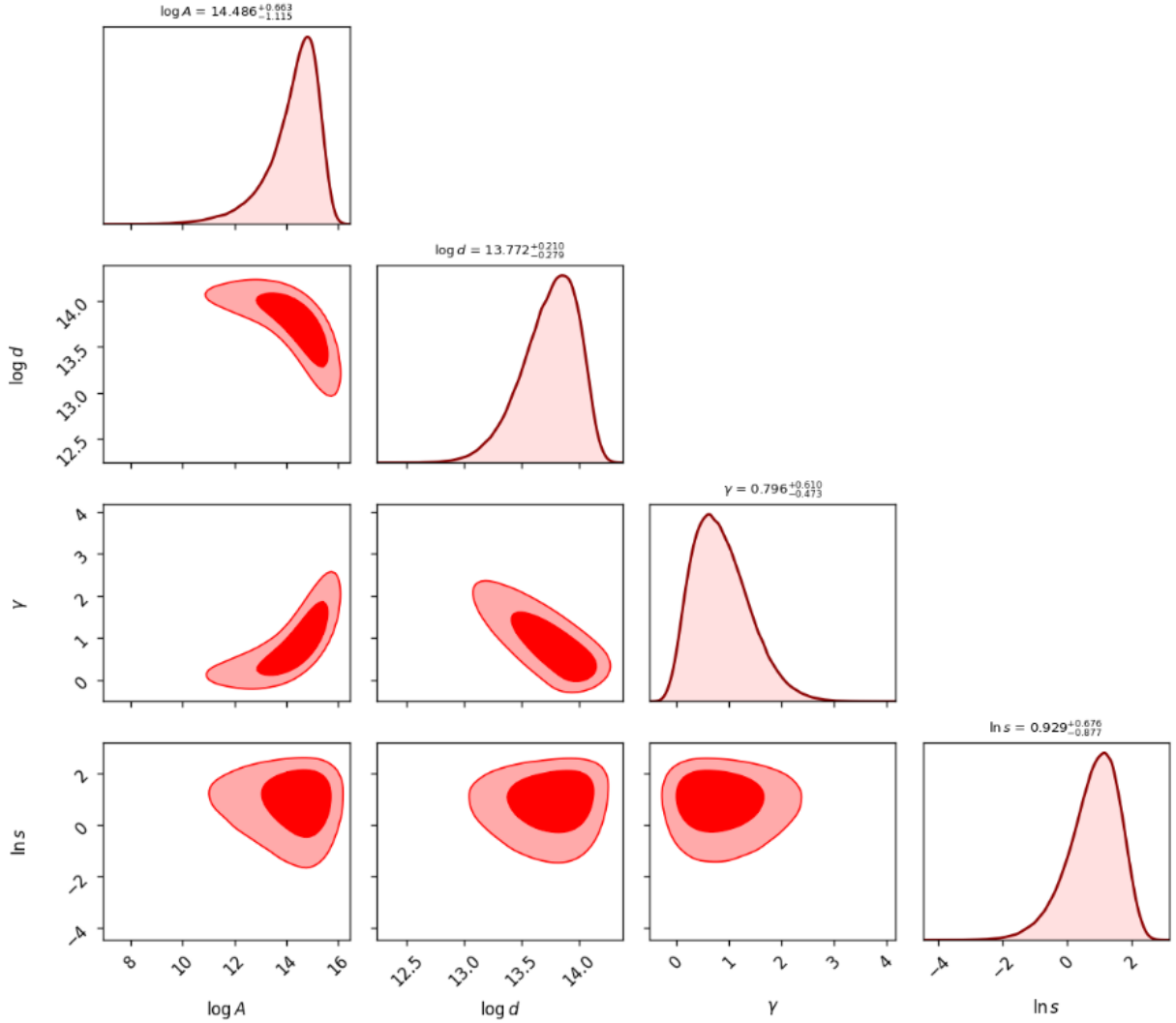


Figure 4: Model(1) Hubble data with four parameter

The Hubble data was used to create contour maps for four parameters ( $\log A$ ,  $\log d$ ,  $\gamma$ ,  $\ln S$ ). The lighter contours show the 95% levels, whereas the darker areas provide the 68% confidence intervals. The most likely estimates are provided by peak values in the diagonal histograms, which display the one dimensional marginalized posterior distributions. Tight constraints on the parameters are shown by the well defined and narrow peaks. Specifically, the expansion redshift dependency is reflected in the conclusion  $\gamma \approx 0.8$  and further data uncertainties are taken into account by the intrinsic scatter parameter  $s$ . These parameter fits, which are confirmed by the AIC and BIC values, show that the four-parameter model outperforms the Elementary constant Hubble model in terms of statistically describing the expansion of the universe.

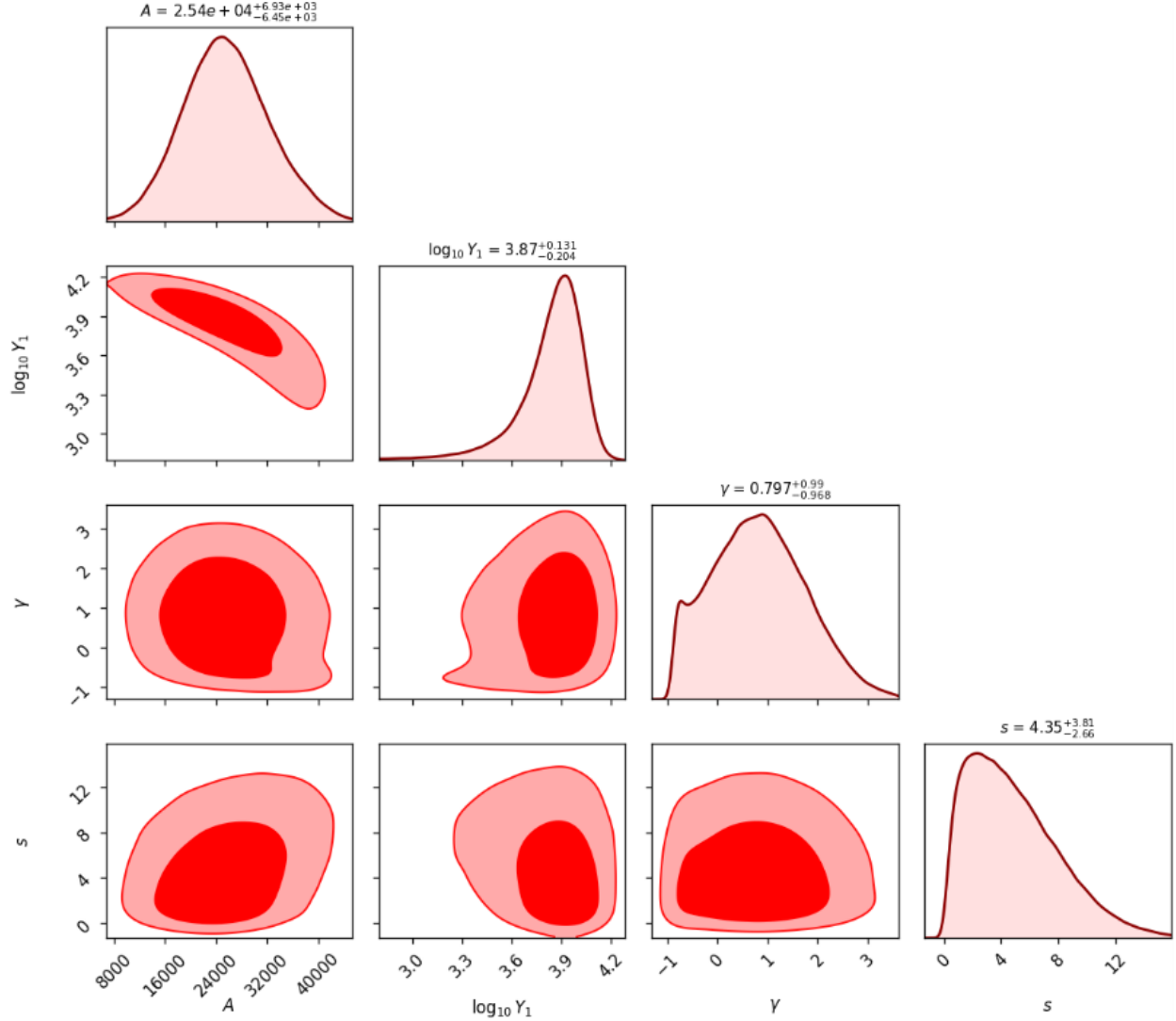


Figure 5: Model(2) Hubble data with four parameter

The joint posteriors are displayed by the contours for  $(A, \log_{10} Y_1, \gamma, s)$ . Light red indicates 95% credibility, dark red 68%. The most likely values are indicated by peaks on the diagonals about  $A \sim 2.5 \times 10^4$ ,  $\log_{10} Y_1 \sim 3.9$ ,  $\gamma \sim 0.8$ ,  $s \sim 4 - 5$ . These parameters are well limited by the Hubble data, as indicated by the thin 1D peaks. The angled ovals that lie between  $\log_{10} A$  and  $\log_{10} Y_1$  show a negative correlation, which is a common degeneracy in expansion models, meaning that raising one can be partially compensated by decreasing the other.

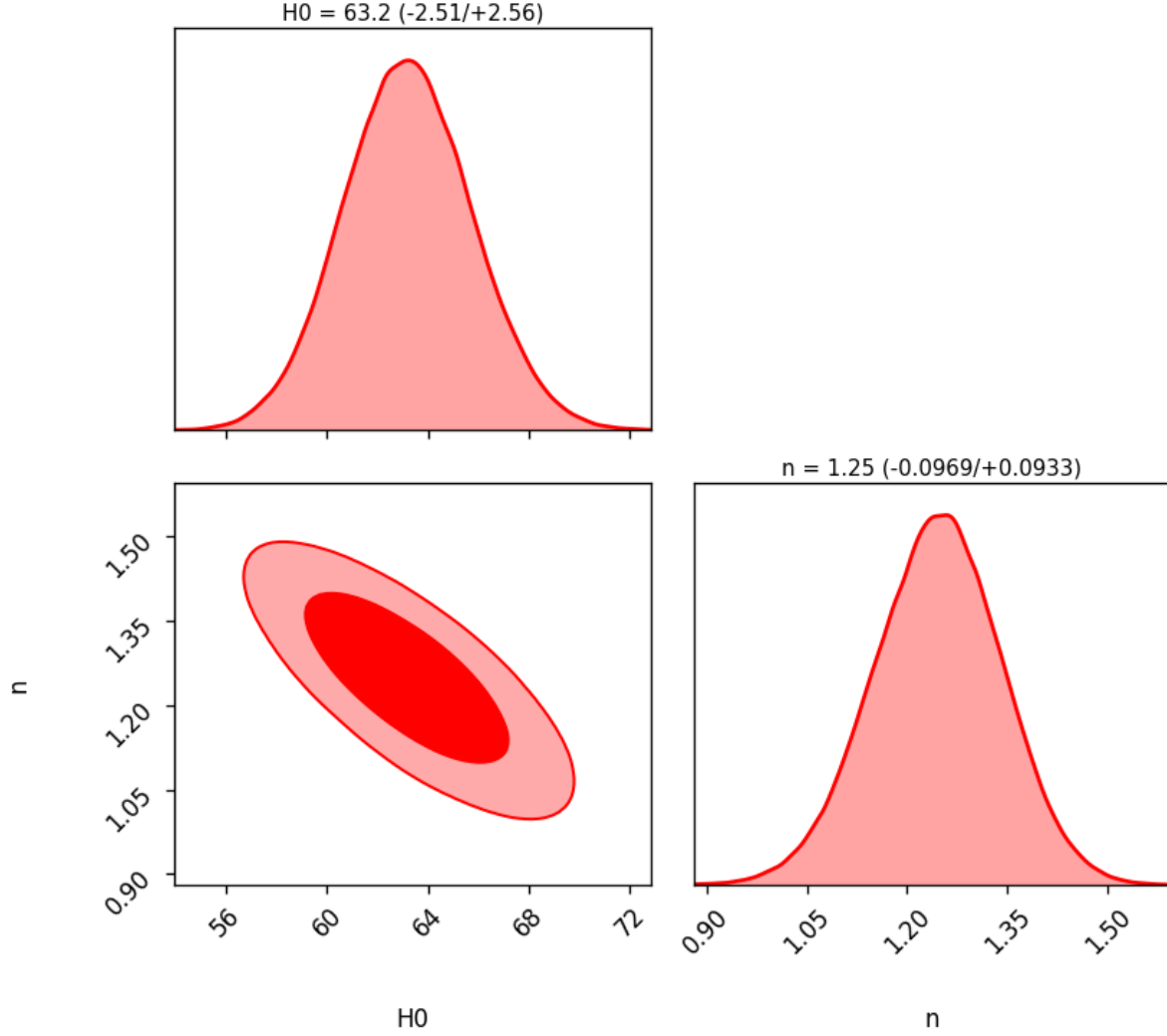


Figure 6: Model(3) Hubble data with two parameter

These contours for  $(H_0, n)$  show the joint posteriors. The 95% credibility region is shown in light red, and the 68% region is shown in dark red. The values that are most likely are shown. with  $H_0 \sim 63.2$  and  $n \sim 1.25$ , by the diagonal peaks. The tight 1D peaks show that these parameters are well restricted by the Hubble data. An rise in  $H_0$  can be partially countered by a drop in  $n$ , a common degeneracy in cosmological expansion models, as seen by the angled ovals between  $H_0$  and  $n$ .

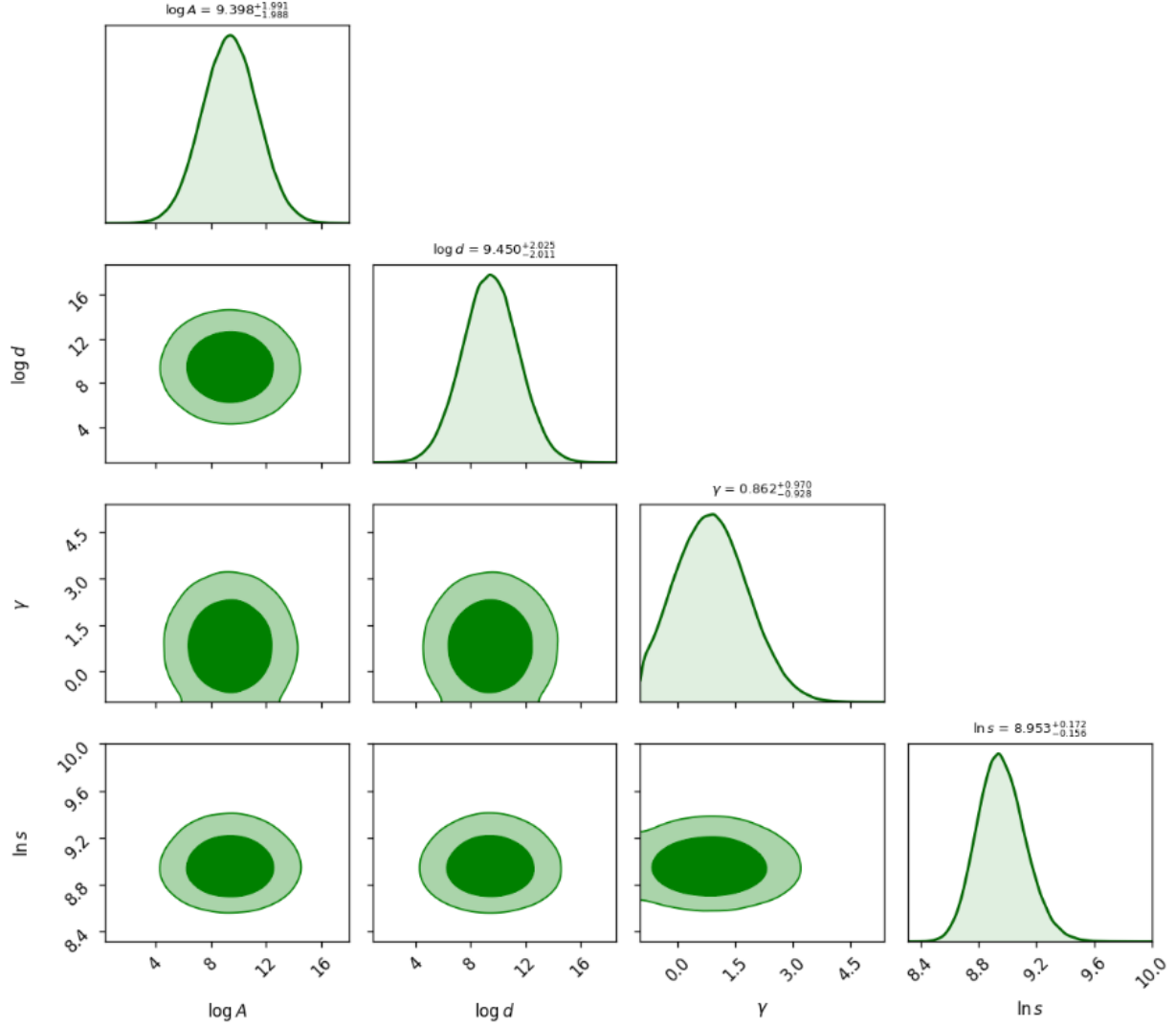


Figure 7: Model(1) BAO data with four parameter

The green contours for  $(\log A, \log d, \gamma, \ln s)$  show the joint posteriors. The 95% credibility region is shown in light green, and the 68% region is shown in dark green. The peaks on the diagonals, which read as follows from the panel titles:  $\log A \approx 9.40$ ,  $\log d \approx 9.45$ ,  $\gamma \approx 0.86$ , and  $\ln s \approx 8.95$ , represent the most likely values. The thin, strongly peaked 1D marginals show that the Hubble data well constrains these parameters. A significant positive correlation, which is a common degeneracy in expansion models where an increase in one parameter can be partially offset by an increase in the other, is indicated by the angled ovals between  $\log A$  and  $\log d$ . Overall, the fit's uncertainties and parameter covariances are summarized by the 68/95% contours.

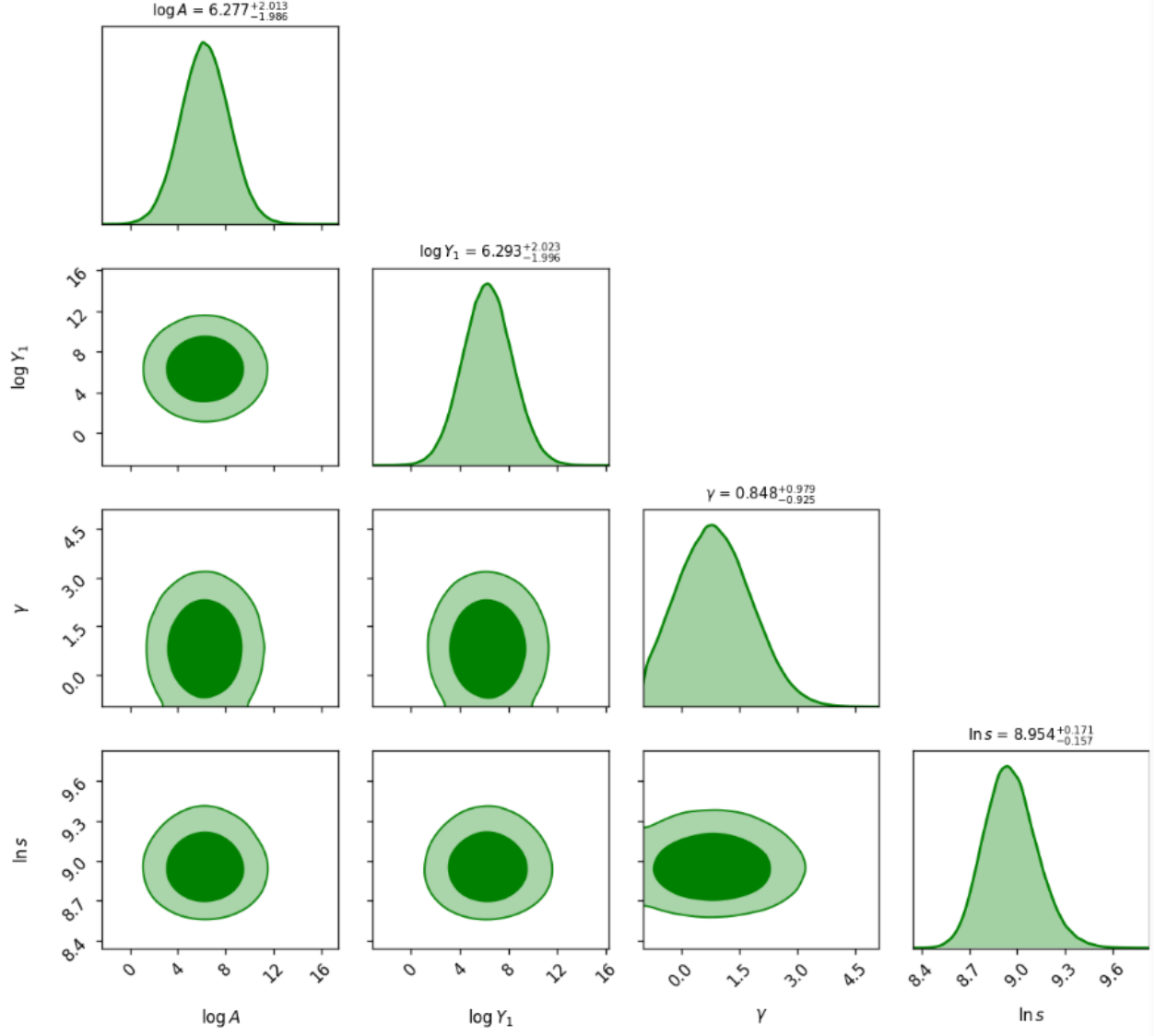


Figure 8: Model(2) BAO data with four parameter

The green contours for  $(\log A, \log Y_1, \gamma, \ln s)$  show the joint posteriors. The 95% credibility region is shown in light green, and the 68% region is shown in dark green. According to the panel titles, the diagonals' peaks show the most likely values:  $\log A \approx 6.28$ ,  $\log Y_1 \approx 6.29$ ,  $\gamma \approx 0.85$ ,  $\ln s \approx 8.95$ . The sharp 1D marginals show that these parameters are generally well constrained by the Hubble data, although  $\gamma$  is still relatively broader. The angled ovals between  $\log A$  and  $\log Y_1$  indicate a moderate positive correlation, a common degeneracy where increasing one may be partly offset by increasing the other, while  $\ln s$  shows weak connection with the other parameters.

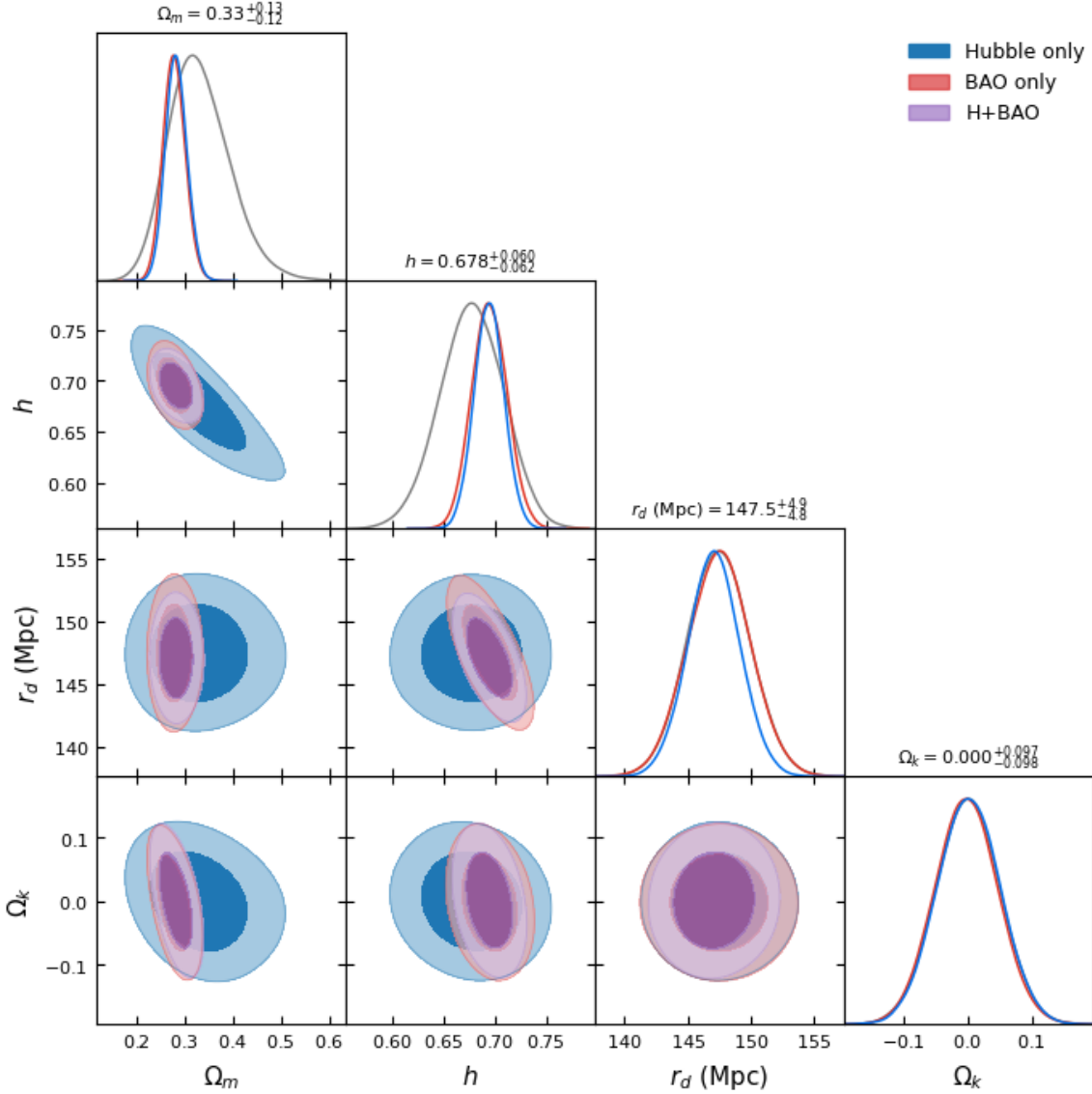


Figure 9:  $\Lambda$ CDM plot with hybrid dataset

The triangle (corner) plot of cosmological parameter constraints derived from three datasets—Hubble-only (blue), BAO-only (red), and the combined **H+BAO** (purple)—is shown in the attached figure. The diagonal panels display the marginalized one-dimensional posterior distributions, while the contours in the two-dimensional parameter spaces correspond to the 68% and 95% confidence levels.  $\Omega_m = 0.3321 \pm 0.0645$ ,  $h = 0.6776 \pm 0.0312$ ,  $r_d = 147.48 \pm 2.47$  Mpc, and  $\Omega_k = 0.00035 \pm 0.0498$  are the mean values for the Hubble-only case, which show very broad uncertainties in comparison to the other datasets. With  $\Omega_m = 0.2790 \pm 0.0231$ ,  $h = 0.6951 \pm 0.0173$ ,  $r_d = 147.49 \pm 2.49$  Mpc, and  $\Omega_k = -0.0021 \pm 0.0492$ , the BAO-only restrictions are more stringent. The degeneracies are greatly decreased when combining Hubble and BAO data, which improves the constraints:  $\Omega_k = 0.0015 \pm 0.0491$ ,  $r_d = 147.09 \pm 2.06$  Mpc,  $h = 0.6947 \pm 0.0145$ , and  $\Omega_m = 0.2833 \pm 0.0224$ . The image makes it evident that the BAO-only dataset gravitates toward lower  $\Omega_m$  and higher  $h$  values, whereas the Hubble-only dataset favors slightly higher  $\Omega_m$  and lower  $h$  values. By balancing these shifts, the joint study produces cosmological parameters that are more accurate and reliable. Stronger restrictions on the cosmic expansion history and curvature are provided by the overlapping contours in the combined case, which demonstrate the complementary nature of the two probes in breaking parameter



degeneracies.

Table 1: Model fits to cosmological data, showing dataset, model name, parameter sets, and best-fit values.

Data used	Model	Parameter	Best-fit value
Hubble	Model 1	$\log A$	14.6618
		$\log d$	13.7294
		$\gamma$	0.8926
		$\ln s$	1.0476
	Model 2	$\log A$	10.1108
		$\gamma$	0.7181
		$\log Y_1$	8.964088
		$s$	4.796930
		$H_0$	63.174
	Model 3	$n$	1.2503
BAO	Model 1	$\log A$	9.4285
		$\log d$	9.5025
		$\gamma$	0.7844
		$\ln s$	8.9461
	Model 2	$A$	471.655
		$Y_1$	547.897
		$\gamma$	0.8096
		$s$	7590.6

Table 2: Model fits to cosmological data, showing dataset, model name and information criteria.

Data used	Model	$\chi^2$	Reduced $\chi^2$	AIC	BIC
Hubble	Model 1	13.6257	0.5047	247.29	252.90
	Model 2	24.0630	0.8912	260.36	265.96
	Model 3	15.8029	0.5644	245.87	250.08
BAO	Model 1	13.5882	0.9706	363.19	366.52
	Model 2	12.3500	0.9500	363.94	367.27

## 5 Hubble and deceleration parameters

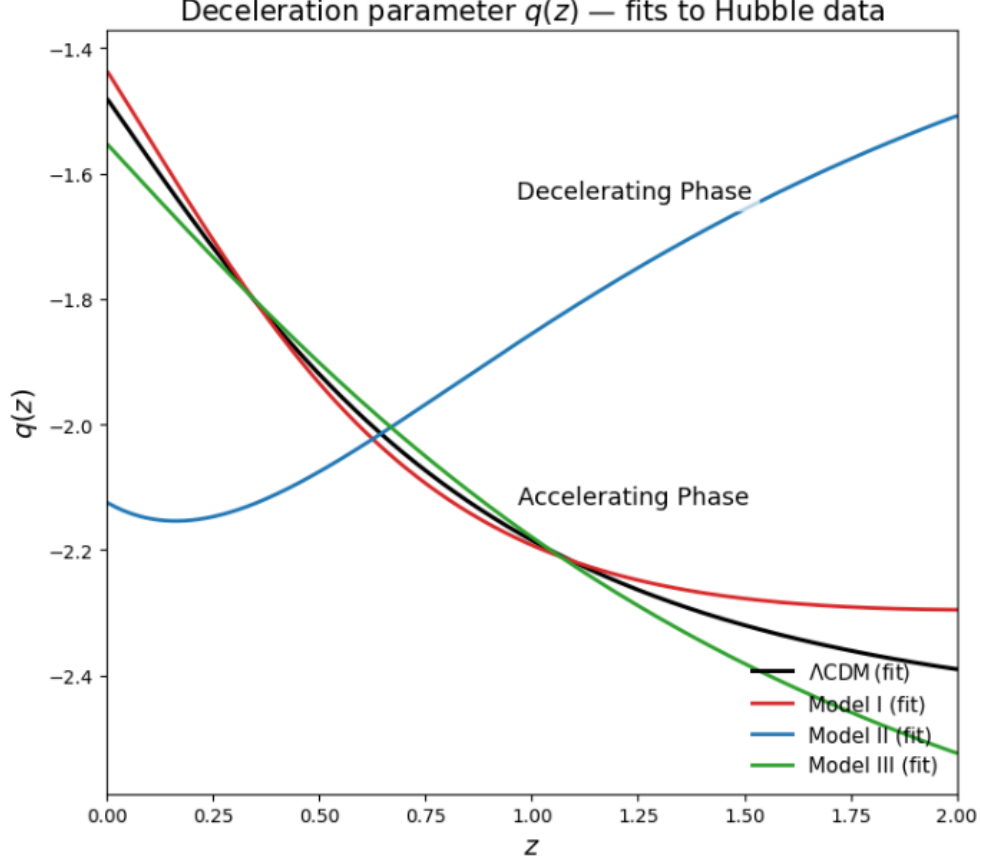


Figure 10: Plot for Hubble and deceleration parameter  $q(z)$

Using the linear-calibration fits  $H_{\text{fit}}(z) = a H_{\text{model}}(z) + b$  reported in the output (Model I:  $a = 132.693869$ ,  $b = -46.507373$ ; Model II:  $a = 73.110226$ ,  $b = -10.257758$ ; Model III:  $a = 25.850453$ ,  $b = 41.733689$ ;  $\Lambda$ CDM fit:  $H_0 = 68.157188$ ,  $\Omega_m = 0.319486$ ), we computed the deceleration parameter from the fitted Hubble functions using

$$q(z) = - \left( 1 + \frac{\dot{H}}{H^2} \right) = -1 - \frac{1+z}{H(z)} \frac{dH}{dz},$$

with  $\frac{dH}{dz}$  evaluated numerically on a fine grid (central differences). Because for the linear calibration  $H_{\text{fit}} = aH + b$  one has  $\frac{dH_{\text{fit}}}{dz} = a \frac{dH}{dz}$ , the fitted  $q$ -formula becomes

$$q_{\text{fit}}(z) = -1 - (1+z) \frac{a H'(z)}{a H(z) + b},$$

Consequently, the calibration shifts the denominator by  $b$  while simultaneously rescaling the derivative. In actuality, the specific  $a, b$  numbers mentioned above do not result in a  $q$  sign change. We examined the displayed range  $0 \leq z \leq 2$  and looked for a root  $q(z) = 0$  on a dense grid up to  $z = 10$ ; numerically, the fitted curves stayed negative everywhere we looked. For comparison, over the depicted interval  $0 \leq z \leq 2$ , the fitted curves provide roughly the following values:  $\Lambda$ CDM:  $q(0) \approx -1.48$ ,  $q(2) \approx -2.18$ ; Model I:  $q(0) \approx -1.44$ ,  $q(2) \approx -2.19$ ; Model II:  $q(0) \approx -2.12$ ,  $q(2) \approx -1.86$ ; Model III:  $q(0) \approx -1.55$ ,  $q(2) \approx -2.18$ . The fitted data show no acceleration-to-deceleration transition (no  $q = 0$  crossing) since all of these values are absolutely negative and no sign change was seen up to  $z = 10$ . Consequently, within the examined redshift range, all theories predict ongoing cosmic acceleration.

## 6 Stability analysis

The effective sound speed is used to analyze the models' dynamical stability and is defined as

$$C_s^2 \equiv \frac{d\bar{p}}{d\rho}, \quad \bar{p} = p - 3\xi H,$$

with the stability

$$C_s^2 \geq 0 \quad (\text{classical stability}),$$

In terms of derivatives,

$$C_s^2 = \frac{dp}{d\rho} - 3\xi \frac{dH}{d\rho}.$$

$C_s^2$  varies with cosmic time  $t$  for three models with bulk viscosity parameter  $\xi = 0.65$

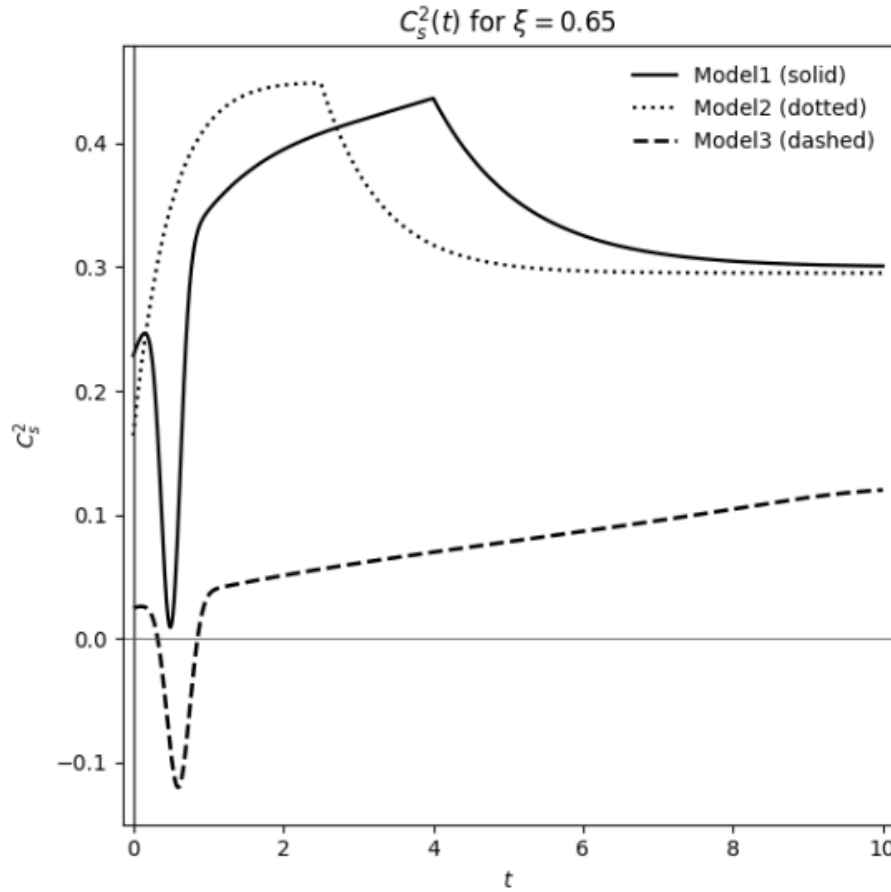


Figure 11: Stability curve for Model (1),(2) and (3)

Since  $C_s^2 > 0$  denotes a stable configuration and  $C_s^2 < 0$  implies instability, Figure 11 shows the evolution of the squared sound speed  $C_s^2(t)$  for the three proposed cosmological models—Model 1 (solid), Model 2 (dotted), and Model 3 (dashed)—at a fixed viscous parameter  $\xi = 0.65$ . This serves as an indicator of their dynamical stability. Model 1 first goes through an oscillating phase, as seen in the picture, with a transient instability ( $C_s^2 < 0$ ) at early times ( $t < 2$ ), before stabilizing around  $C_s^2 \approx 0.3$  over time. The strongest and most reliable stability of the three is shown by Model 2, which stays positive for the most of its history, peaking close to  $t \approx 3$  and then moving toward a steady constant value. Model 3, on the other hand, begins with an unstable phase ( $C_s^2 < 0$ ) around  $t \approx 1$  and then progressively moves into a positive

regime, eventually reaching  $C_s^2 \approx 0.1$ . While Model 2 exhibits the highest level of stability, Model 1 achieves stability following early oscillations, and Model 3 stabilizes more slowly, all three models generally evolve toward stable configurations in the late universe. This indicates that the cosmological dynamics in each case asymptotically approach stable behavior at late cosmic times.

## 7 Conclusion

In this work, we have explored the dynamics of a bulk viscous cosmological model within the Friedmann–Robertson–Walker (FRW) spacetime framework, where the cosmic fluid obeys a nonlinear equation of state that unifies dark energy and dark matter behavior. The presence of bulk viscosity was incorporated into the Friedmann equations, modifying the background dynamics and influencing the Universe’s late-time acceleration. Analytical solutions for the energy density and Hubble parameter were obtained for different cases of the viscous coefficient, and these solutions were further examined through stability analysis and confrontation with observational data.

Our results show that the inclusion of a bulk viscous term plays a significant role in describing the accelerated expansion of the Universe without invoking an explicit cosmological constant. The derived expressions for the Hubble and deceleration parameters illustrate a smooth transition from an early decelerated phase to a late-time accelerated regime, consistent with modern observational evidence. Moreover, the effective sound speed analysis confirms that the proposed models remain dynamically stable and causal over the entire evolutionary range considered.

From the observational perspective, the models were tested using Hubble parameter (OHD) and baryon acoustic oscillation (BAO) datasets, constrained through a Markov Chain Monte Carlo (MCMC) approach. The results demonstrate strong consistency with  $\Lambda$ CDM trends while allowing controlled deviations that may offer deeper insights into the physics of dissipative processes in the cosmic medium. The goodness-of-fit statistics, including the reduced  $\chi^2$ , AIC, and BIC values, confirm that the viscous models provide a competitive description of the observed expansion history.

The statistical contours from the MCMC analysis also highlight well-defined parameter regions, revealing that the viscosity coefficient  $\xi$  and the equation of state parameter  $\gamma$  are tightly constrained by current data. This indicates that the bulk viscous framework is not only phenomenologically viable but also capable of capturing essential features of cosmic acceleration within a unified dark sector description.

For future research, several extensions of this work are promising. It would be valuable to generalize the analysis to non-flat universes ( $k \neq 0$ ) and to consider a time-dependent or scale-dependent bulk viscosity coefficient. Additionally, studying the thermodynamic properties and entropy evolution in such viscous cosmologies could further illuminate the connection between cosmic expansion and gravitational thermodynamics. Another potential direction involves exploring the implications of these models in alternative gravity theories, such as  $f(R)$ ,  $f(Q, T)$ , or mimetic gravity, where dissipative effects could arise naturally from modified geometric frameworks. Finally, confronting these extended viscous models [14] with next-generation observational data, including CMB anisotropies and large-scale structure surveys, would provide a more robust test of their physical validity.

In summary, our findings reinforce the importance of bulk viscous cosmology as a compelling approach to explain the late-time acceleration of the Universe. By combining analytical modeling, dynamical stability analysis, and statistical inference with observational data, this study contributes to a deeper understanding of how dissipative processes can shape the evolution of the cosmic fluid and provide an alternative pathway to dark energy phenomenology.

## Data Availability statement

This research did not yield any new data.

## Conflict of Interest

Authors declare there is no conflict of interest.

## Funding

This work was supported by the Deanship of Scientific Research, Vice Presidency for Graduate Studies and Scientific Research, King Faisal University, Saudi Arabia (KFU253534).

## Acknowledgments

PKD would like to thank the Isaac Newton Institute for Mathematical Sciences, Cambridge, for support and hospitality during the programme Statistical mechanics, integrability and dispersive hydrodynamics where work on this paper was undertaken. This work was supported by EPSRC grant no EP/K032208/1. Also, PKD wishes to acknowledge that part of the numerical computation of this work was carried out on the computing cluster Pegasus of IUCAA, Pune, India and PKD gratefully acknowledges Inter-University Centre for Astronomy and Astrophysics (IUCAA), Pune, India for providing them a Visiting Associateship under which a part of this work was carried out.

## References

- [1] Alijanzadeh Boura, H., Sadeghi, J.: 2025, The Modified Chaplygin Gas and Dark Degeneracy with Phantom Model, *Journal of Holography Applications in Physics* 5(1), 108-122.  
<https://doi.org/10.22128/jhap.2025.949.1109>
- [2] Bali, R., Dave, S.: 2002, Bianchi Type-III String Cosmological Model with Bulk Viscous Fluid in General Relativity, *Astrophysics and Space Science* 282, 461–466.  
<https://doi.org/10.1023/A:1020834610024>
- [3] Bamba, K., Capozziello, S., Nojiri, S. et al.: 2012, Dark energy cosmology: the equivalent description via different theoretical models and cosmography tests, *Astrophys Space Sci* 342, 155–228 .  
<https://doi.org/10.1007/s10509-012-1181-8>
- [4] Bandyopadhyay, T.: 2012, Thermodynamics of Gauss-Bonnet brane with modified Chaplygin gas, *Astrophys Space Sci* 341, 689–693. <https://doi.org/10.1007/s10509-012-1115-5>
- [5] Banerjee, A., Bhui, B. & Chatterjee, S.: 1990, Bianchi type I cosmological models in higher dimensions, *Astrophysical Journal, Part 1 (ISSN 0004-637X)*, vol. 358, July 20, 1990, p. 23-27. Research supported by the Council for Scientific and Industrial Research and UGCI, 358, 23-27.  
[https://ui.adsabs.harvard.edu/link\\_gateway/1990ApJ...358...23B/doi:10.1086/168959](https://ui.adsabs.harvard.edu/link_gateway/1990ApJ...358...23B/doi:10.1086/168959)
- [6] Benaoum, H.: 2022, Accelerated universe from modified Chaplygin gas and tachyonic fluid, *Universe*, 8(7), 340.  
<https://doi.org/10.3390/universe8070340>
- [7] Bennet, C. L.: 2003, The Third Data Release of the Sloan Sky Survey, *Astrophysical Journal Supplement Ser*, 148, 97-117.  
<https://doi.org/10.1086/427544>
- [8] Brevik, I., Grøn, Ø., de Haro, J., Odintsov, S. D., & Saridakis, E. N.: 2017, Viscous cosmology for early-and late-time universe, *International Journal of Modern Physics D*, 26(14), 1730024.  
<https://doi.org/10.1142/S0218271817300245>
- [9] Brevik, I., Elizalde, E., Nojiri, S. I., & Odintsov, S. D.: 2011, Viscous little rip cosmology, *Physical Review D—Particles, Fields, Gravitation, and Cosmology*, 84(10), 103508.  
<https://doi.org/10.1103/PhysRevD.84.103508>
- [10] Caldwell, R.: 2002, A phantom menace? Cosmological consequences of a dark energy component with super-negative equation of state, *Physics Letters B*, 545(1-2), 23-29.  
[https://doi.org/10.1016/S0370-2693\(02\)02589-3](https://doi.org/10.1016/S0370-2693(02)02589-3)

- [11] Carroll, S.M.: 2001, The Cosmological Constant, *Living Rev. Relativ*, 4, 1 .  
<https://doi.org/10.12942/lrr-2001-1>
- [12] Chatterjee, S., Bhui, B.: 1990, Viscous fluid in a kaluza-klein metric, *Astrophys Space Sci* 167, 61–67 .  
<https://doi.org/10.1007/BF00642063>
- [13] Debnath, U., Banerjee, A., & Chakraborty, S.: 2004, Role of modified Chaplygin gas in accelerated universe, *Classical and Quantum Gravity*, 21(23), 5609.  
<https://doi.org/10.1088/0264-9381/21/23/019>
- [14] Dhankar, P. K., Munyeshyaka, A., Sanyal, A., Islam, S., & Rahaman, F.: 2025, Constraints on multi-fluid cosmology in modified Gauss-Bonnet gravity models with different observational data sets, ArXiv.  
<https://arxiv.org/abs/2507.22191>
- [15] Dhankar, P. K., Mhamdi, D., Munyeshyaka, A., Kumar, D., Ntahompagaze, J., & Ouali, T.: 2025, Testing Gauss-Bonnet Gravity with DESI BAO Data, ArXiv.  
<https://arxiv.org/abs/2508.03602>
- [16] Dhankar, P. K., Munyeshyaka, A., Hussain, S., & Mutabazi, T.: 2025, Large scale structure constraints and matter power spectrum in  $f(Q, \mathcal{L}_m)$  gravity, ArXiv.  
<https://arxiv.org/abs/2507.10631>
- [17] Dhankar, P. K., Sanyal, A., Munyeshyaka, A., Ray, S., & Pourhassan, B.: 2025, Observational analysis of bulk viscous modified Chaplygin gas in (2+1)dimensional universe using MCMC, ArXiv.  
<https://arxiv.org/abs/2504.18612>
- [18] Dhankar, P. K., Islam, S., Ray, S., Sanyal, A., & Maurya, S. K.: 2025, Observational constraints on holography in  $(2 + 1)$ -dimensional cosmology with a generalized equation of state, ArXiv.  
<https://arxiv.org/abs/2508.11701>
- [19] Dhankar, P. K.: 2018, Frw bulk viscous cosmology with modified chaplygin gas in flat space in  $(2+1)$ -dimensional spacetime.
- [20] Dhankar, P. K., Sanyal, A., Islam, S., Rahaman, F., & Pourhassan, B.: 2025, Testing the Generalized Second Law in  $(2 + 1)$ -Dimensional Cosmology: Holographic Entropy Bounds and Observational Constraints, ArXiv.  
<https://arxiv.org/abs/2508.13227>
- [21] Feng, B., Wang, X., & Zhang, X.: 2005, Dark energy constraints from the cosmic age and supernova, *Physics Letters B*, 607(1-2), 35-41.  
<https://doi.org/10.1016/j.physletb.2004.12.071>
- [22] Feroz, F., & Hobson, M. P.: 2008, Multimodal nested sampling: An efficient and robust alternative to Markov Chain Monte Carlo methods for astronomical data analyses, *Monthly Notices of the Royal Astronomical Society*, 384(2), 449-463.  
<https://doi.org/10.1111/j.1365-2966.2007.12353.x>
- [23] Gadbail, G. N., Arora, S., Kumar, P., & Sahoo, P.: 2022, Interaction of divergence-free deceleration parameter in Weyl-type  $f(Q,T)$  gravity, *Chinese Journal of Physics*, 79, 246-255.  
<https://doi.org/10.1016/j.cjph.2022.09.005>
- [24] Georgiev, S. G., Khadekar, G., & Kumar, P.: 2020, Two dimensional integral inequalities on time scales, arXiv preprint arXiv:2003.05309.  
<https://doi.org/10.48550/arXiv.2003.05309>
- [25] Guo, Z., Piao, Y., Zhang, X., & Zhang, Y.: 2005, Cosmological evolution of a quintom model of dark energy, *Physics Letters B*, 608(3-4), 177-182.  
<https://doi.org/10.1016/j.physletb.2005.01.017>

- [26] Ibotombi Singh, N., Romaleima Devi, S.: 2011, A new class of bulk viscous FRW cosmological models in a scale covariant theory of gravitation, *Astrophys Space Sci* 334, 231–236 .  
<https://doi.org/10.1007/s10509-011-0739-1>
- [27] Islam, S., Dhankar, P. K., Thakran, B., & Kumbhare, S. R.: 2024, String Cloud with quark matter and viscous fluid admitting conformal motion, *Romanian Astronomical Journal*, Vol. 34, Nos. 1-2, p. 15–32.  
<https://doi.org/10.59277/RoAJ.2023.1-2.02>
- [28] Islam, S., Kumar, P., Khadekar, G. S., & Das, T. K.: 2019, (2+ 1) dimensional cosmological models in  $f(R, T)$  gravity with  $(R, T)$ , In *Journal of Physics: Conference Series* (Vol. 1258, No. 1, p. 012026). IOP Publishing.  
<https://doi.org/10.1088/1742-6596/1258/1/012026>
- [29] Islam, S., & Kumar, P.: 2021, Gravitational model of compact spherical reissner-nordström-type star under  $f(r, t)$  gravity, *Journal of Dynamical Systems and Geometric Theories*, 19(1), 135-154.  
<https://doi.org/10.1080/1726037X.2021.1965705>
- [30] Jamil, M., Momeni, D., Serikbayev, N.S. et al.: 2012, FRW and Bianchi type I cosmology of f-essence, *Astrophys Space Sci* 339, 37–43 .  
<https://doi.org/10.1007/s10509-011-0964-7>
- [31] Joshi, S., Dhankar, P. K., Islam, S., & Deo, S. D.: 2025, Exploring Bianchi Types Cosmological Models in the Framework of Modified- $f(R)$  Gravity, *Romanian Astronomical Journal*, 35(1-2), 15-36.  
<https://doi.org/10.59277/RoAJ.2025.1-2.02>
- [32] Katore, S.D., Shaikh, A.Y., Kapse, D.V. et al.: 2011, FRW Bulk Viscous Cosmology in Multi Dimensional Space-Time, *Int J Theor Phys* 50, 2644–2654 .  
<https://doi.org/10.1007/s10773-011-0760-8>
- [33] Khadekar, G., Ray, S., Sanyal, A., & Dhankar, P. K.: 2025, Holographic principle inspired dark energy description of unified early and late universe in viscous mimetic gravity, *Physics of the Dark Universe*, 47, 101742.  
<https://doi.org/10.1016/j.dark.2024.101742>
- [34] Khadekar, G.S., Kumar, P. & Islam, S.: 2019, Modified Chaplygin gas with bulk viscous cosmology in FRW (2+1)-dimensional spacetime, *J Astrophys Astron* 40, 40 .  
<https://doi.org/10.1007/s12036-019-9606-1>
- [35] Knop, R. A., Aldering, G., Amanullah, R., Astier, P., Blanc, G., Burns, M. S.,: 2003,... & Supernova Cosmology Project: New constraints on  $\Omega$ ,  $\Lambda$ , and  $w$  from an independent set of 11 high-redshift supernovae observed with the Hubble Space Telescope, *The Astrophysical Journal*, 598(1), 102.  
<https://doi.org/10.1086/378560>
- [36] Khadekar, G. S., Gupta, A., & Pande, K.: 2019, FRW viscous modified cosmic Chaplygin gas cosmology in the presence of cosmological constant, *International Journal of Geometric Methods in Modern Physics*, 16(09), 1950141.  
<https://doi.org/10.1142/S021988781950141X>
- [37] Kumar, P., & Khadekar, G.: 2021, Holographic Dark Energy with Modified Chaplygin Gas and Scalar Field in (2 + 1)-Dimensional Space-time, *Journal of the Tensor Society*, 15(01), 17-44.  
<https://doi.org/10.56424/jts.v15i01.10615>
- [38] Kumar, P., Khadekar, G. S., & Dagwal, V. J.: 2022, Two fluids cosmological model in (2+ 1)-dimensional saez-ballester scalar-tensor theory of gravitation, *Journal of Dynamical Systems and Geometric Theories*, 20(1), 91-114.  
<https://doi.org/10.1080/1726037X.2022.2079267>

- [39] Kumar, D., Dhankar, P. K., Ray, S., & Zhang, F.: 2025, Joint analysis of constraints on  $f(R)$  parametrization from recent cosmological observations, *Physics of the Dark Universe*, 49, 101989.  
<https://doi.org/10.1016/j.dark.2025.101989>
- [40] Kumbhare, S. R., Kumar, P., & Islam, S.: 2022, Strange Quark Matter attached to String Cloud in General Relativity under 5D space-time, *Journal of the Tensor Society*, 16(01), 81-92.  
<https://doi.org/10.56424/jts.v16i01.194>
- [41] Mazumder, N., Biswas, R. & Chakraborty, S.: 2012, FRW Cosmological Model with Modified Chaplygin Gas and Dynamical System, *Int J Theor Phys* 51, 2754–2758 .  
<https://doi.org/10.1007/s10773-012-1150-6>
- [42] Misner, C. W.: 1968, The isotropy of the universe, *Astrophysical Journal*, vol. 151, p. 431, 151, 431.  
<https://doi.org/10.1086/149448>
- [43] Moresco, M.: 2015, Raising the bar: new constraints on the Hubble parameter with cosmic chronometers at  $z \sim 2$ , *Monthly Notices of the Royal Astronomical Society: Letters*, 450(1), L16-L20.  
<https://doi.org/10.1093/mnrasl/slv037>
- [44] Mune, M., Dhankar, P. K., Islam, S., Pourhassan, B., Aamir, M., & Haroon, F.: 2025, Statistical Constraints on Anisotropic Bianchi-III Cosmology in  $f(R, T)$ -Gravity Using MCMC Methods, ArXiv.  
<https://arxiv.org/abs/2510.19852>
- [45] Munyeshyaka, A., Dhankar, P. K., & Ntahompagaze, J.: 2024, Perturbations with bulk viscosity in modified chaplygin gas cosmology, ArXiv.  
<https://doi.org/10.1142/S0219887825500732>
- [46] Munyeshyaka, A., Dhankar, P. K., & Ntahompagaze, J.: 2025, Matter power spectrum in a power-law  $f(G)$  gravity, *New Astronomy*, 120, 102423.  
<https://doi.org/10.1016/j.newast.2025.102423>
- [47] Murphy, G. L.: 1973, Big-bang model without singularities, *Physical Review D*, 8(12), 4231.  
<https://doi.org/10.1103/PhysRevD.8.4231>
- [48] Nobbenhuis, S.: 2006, Categorizing Different Approaches to the Cosmological Constant Problem, *Found Phys* 36, 613–680 .  
<https://doi.org/10.1007/s10701-005-9042-8>
- [49] Nojiri, S. I., & Odintsov, S. D.: 2005, Inhomogeneous equation of state of the universe: Phantom era, future singularity, and crossing the phantom barrier, *Physical Review D—Particles, Fields, Gravitation, and Cosmology*, 72(2), 023003.  
<https://doi.org/10.1103/PhysRevD.72.023003>
- [50] Padmanabhan, T.: 2003, Cosmological constant—The weight of the vacuum, *Physics Reports*, 380(5-6), 235-320.  
[https://doi.org/10.1016/S0370-1573\(03\)00120-0](https://doi.org/10.1016/S0370-1573(03)00120-0)
- [51] Panda, A., Manna, G., Ray, S., Khlopov, M., & Dhankar, P. K.: 2024, Thermodynamics of a Non-canonical  $f(R, T)$  gravity, *Physics of the Dark Universe*, 46, 101697.  
<https://doi.org/10.1016/j.dark.2024.101697>
- [52] Paul, T.: 2025, Origin of bulk viscosity in cosmology and its thermodynamic implications, *Physical Review D*, 111(8), 083540.  
<https://doi.org/10.1103/PhysRevD.111.083540>
- [53] Peebles, P. J. E., & Ratra, B.: 1988, Cosmology with a time-variable cosmological 'constant', *Astrophysical Journal, Part 2-Letters to the Editor (ISSN 0004-637X)*, vol. 325, Feb. 15, 1988, p. L17-L20. NSF-supported research., 325, L17-L20.  
[https://ui.adsabs.harvard.edu/link\\_gateway/1988ApJ...325L..17P/doi:10.1086/185100](https://ui.adsabs.harvard.edu/link_gateway/1988ApJ...325L..17P/doi:10.1086/185100)



- [54] Peebles, P. J. E., & Ratra, B.: 2003, The cosmological constant and dark energy, *Reviews of modern physics*, 75(2), 559.  
<https://doi.org/10.1103/RevModPhys.75.559>
- [55] Perlmutter, S., Aldering, G., Goldhaber, G., Knop, R. A., Nugent, P., Castro, P. G.,: 1999, & Supernova Cosmology Project.: Measurements of  $\omega$  and  $\Lambda$  from 42 high-redshift supernovae, *The Astrophysical Journal*, 517(2).  
<https://doi.org/10.1086/307221>
- [56] Pourhassan, B.: 2013, Viscous Modified Cosmic Chaplygin Gas Cosmology, *International Journal of Modern Physics D* Vol. 22, No. 9.  
<https://doi.org/10.1142/S0218271813500612>
- [57] Ratra, B., & Peebles, P. J.: 1988, Cosmological consequences of a rolling homogeneous scalar field, *Physical Review D*, 37(12), 3406.  
<https://doi.org/10.1103/PhysRevD.37.3406>
- [58] Riess, A. G., Filippenko, A. V., Challis, P., Clocchiatti, A., Diercks, A., Garnavich, P. M., ... & Tonry, J.: 1998, Observational evidence from supernovae for an accelerating universe and a cosmological constant, *The astronomical journal*, 116(3). 1009.  
<https://doi.org/10.1086/300499>
- [59] Riess, A. G., Strolger, L. G., Tonry, J., Casertano, S., Ferguson, H. C., Mobasher, B., ... & Tsvetanov, Z.: 2004, Type Ia supernova discoveries at  $z \lesssim 1$  from the Hubble Space Telescope: Evidence for past deceleration and constraints on dark energy evolution, *The Astrophysical Journal*, 607(2), 665.  
<https://doi.org/10.1086/383612>
- [60] Rudra, P.: 2012, Dynamics of interacting generalized cosmic Chaplygin gas in brane-world scenario, *Astrophys Space Sci* 342, 579–599 .  
<https://doi.org/10.1007/s10509-012-1198-z>
- [61] Rudra, P.: Debnath, U. & Biswas, R.: 2012, Dynamics of modified Chaplygin gas in brane world scenario: phase plane analysis, *Astrophys Space Sci* 339, 53–64 .  
<https://doi.org/10.1007/s10509-011-0967-4>
- [62] Saadat, H., Pourhassan, B.: 2013, FRW bulk viscous cosmology with modified Chaplygin gas in flat space, *Astrophys Space Sci* 343, 783–786 .  
<https://doi.org/10.1007/s10509-012-1268-2>
- [63] Saadat, H., Pourhassan, B.:2013, FRW bulk viscous cosmology with modified cosmic Chaplygin gas, *Astrophys Space Sci* 344, 237–241.  
<https://doi.org/10.1007/s10509-012-1301-5>
- [64] Saadat, H.: 2012, FRW Bulk Viscous Cosmology in Non-flat Universe, *Int J Theor Phys* 51, 1317–1322.  
<https://doi.org/10.1007/s10773-011-1007-4>
- [65] Sadeghi, J., Setare, M. R., Amani, A. R., & Noorbakhsh, S. M.:2010, Bouncing universe and reconstructing vector field, *Physics Letters B*, 685(4-5), 229-234.  
<https://doi.org/10.1016/j.physletb.2010.01.071>
- [66] Saha, B., Amirhashchi, H. & Pradhan, A.: 2012, Two-fluid scenario for dark energy models in an FRW universe-revisited, *Astrophys Space Sci* 342, 257–267 .  
<https://doi.org/10.1007/s10509-012-1155-x>
- [67] Samanta, B., Rahaman, F., Raychaudhuri, B., & Dhankar, P. K.: 2025, Tachyonic field coupled with global monopole in Brans-Dicke theory, *Physica Scripta*, 100(7), 075027.  
<https://doi.org/10.1088/1402-4896/ade63c>

- [68] Sanyal, A., Dhankar, P. K., Munyeshyaka, A., Islam, S., & Rahaman, F.: 2025, Cosmic Hysteresis in Reconstructed  $f(R)$  Bounce Models: A Thermodynamic Study, ArXiv.  
<https://arxiv.org/abs/2508.06590>
- [69] Sen, A.: 2002, Tachyon matter, *Journal of High Energy Physics*, 2002(07), 065.  
<https://doi.org/10.1088/1126-6708/2007/05/035>
- [70] Setare, M. R., & Sheykhi, A.: 2010, Thermodynamics of viscous dark energy in an RSII braneworld, *International journal of Modern physics D*, 19(02), 171-181.  
<https://doi.org/10.1142/S0218271810016361>
- [71] Setare, M. R.: 2009, Holographic chaplygin DGP cosmologies, *International Journal of Modern Physics D*, 18(03), 419-427.  
<https://doi.org/10.1142/S0218271809014558>
- [72] Setare, M.: 2007, Interacting generalized Chaplygin gas model in non-flat universe, *Eur. Phys. J. C* 52, 689–692.  
<https://doi.org/10.1140/epjc/s10052-007-0405-5>
- [73] Setare, M.: 2007, Holographic Chaplygin gas model, *Physics Letters B*, 648(5-6), 329-332.  
<https://doi.org/10.1016/j.physletb.2007.03.025>
- [74] Setare, M.: 2007, Interacting holographic generalized Chaplygin gas model, *Physics Letters B*, 654(1-2), 1-6.  
<https://doi.org/10.1016/j.physletb.2007.08.038>
- [75] Singh, G.P., Kale, A.Y.: 2011, Anisotropic bulk viscous cosmological models with particle creation, *Astrophys Space Sci* 331, 207–219 .  
<https://doi.org/10.1007/s10509-010-0400-4>
- [76] Singh, G.P., Deshpande, R.V. & Singh, T.: 2004, Higher-dimensional cosmological model with variable gravitational constant and bulk viscosity in Lyra geometry, *Pramana - J Phys* 63, 937–945.  
<https://doi.org/10.1007/BF02704332>
- [77] Talole, R., Kumar, P., & Islam, S.: 2023, Viscous Modified Ghost Scalar Field Dark Energy Models with Varying  $G$ , *Romanian Astronomical Journal*, 33, 81-109.  
<https://doi.org/10.59277/RoAJ.2023.1-2.06>
- [78] Thakran, B., Dhankar, P. K., Raut, S., Ray, S., Maurya, S. K., & Sanyal, A.: 2025, Cosmological constraints on interacting holographic dark energy and extended Chaplygin gas in using MCMC analysis, *International Journal of Geometric Methods in Modern Physics*.  
<https://doi.org/10.1142/S0219887825502548>
- [79] Turner, M. S., & White, M.: 1997, CDM models with a smooth component, *Physical Review D*, 56(8), R4439.  
<https://doi.org/10.1103/PhysRevD.56.R4439>
- [80] Wei, H., & Cai, R. G.: 2005, Cosmological evolution of “hessence” dark energy and avoidance of the big rip, *Physical Review D—Particles, Fields, Gravitation, and Cosmology*, 72(12), 123507.  
<https://doi.org/10.1103/PhysRevD.72.123507>
- [81] Wei, H., Tang, N., & Zhang, S. N.: 2007, Reconstruction of hessence dark energy and the latest type Ia supernovae gold dataset, *Physical Review D—Particles, Fields, Gravitation, and Cosmology*, 75(4), 043009.  
<https://doi.org/10.1103/PhysRevD.75.043009>
- [82] Weinberg, S.: 1989, The cosmological constant problem, *Reviews of modern physics*, 61(1), 1.  
<https://doi.org/10.1103/RevModPhys.61.1>

- [83] Xu, Y.D., Huang, Z.G. & Zhai, X.H.: 2012, A new type of interaction between generalized Chaplygin gas and dark matter, *Astrophys Space Sci* 339, 31–36 .  
<https://doi.org/10.1007/s10509-012-0974-0>
- [84] Yu, H., Ratra, B., & Wang, F. Y.: 2018, Hubble parameter and Baryon Acoustic Oscillation measurement constraints on the Hubble constant, the deviation from the spatially flat  $\Lambda$ CDM model, the deceleration–acceleration transition redshift, and spatial curvature, *The Astrophysical Journal*, 856(1), 3.  
<https://doi.org/10.3847/1538-4357/aab0a2>